AIAA JOURNAL
Vol. 31, No. 5, May 1993

Common Vortical Structure of Turbulent Flows over Smooth and Rough Boundaries

A. J. Grass,* R. J. Stuart,† and M. Mansour-Tehrani‡
University College London, London, England, United Kingdom

The bursting phenomenon is a common feature of turbulent boundary layers irrespective of the wall roughness condition. Consistent with Theodorsen's conjecture, recent direct numerical simulation studies have shown that the dynamics of this bursting process over smooth walls is directly linked to the presence of powerful vortical structures with a general horseshoe-type configuration. The present paper describes the results of physical experiments that demonstrate that these vortex structures are also present in turbulent boundary layers over rough walls. They appear to form the central element in a recurring, highly nonlinear cycle of turbulence and burst generating instability. Novel velocity measurement techniques were used in the investigation that, for the first time in physical experimental fluid mechanics research, allowed quasi-instantaneous vortex lines to be traced through a three-dimensional block of flow space to reveal the vortical structures embedded in the shear flowfield. Preliminary test results are also presented that indicate that, as in the smooth wall case, the instability structures over rough boundaries have a preferred spanwise wavelength that scales with the roughness dimension.

Introduction

KLINE et al.[1] gave a detailed description of the streaky nature of the flow structure in the viscous sublayer on a smooth wall with its alternating narrow, elongated zones of high and low fluid velocity. They linked this streaky structure to the bursting process that they described as a randomly occurring event comprising gradual local liftup of the fluid in the low-speed streaks, sudden oscillation, bursting, and ejection. This bursting and ejection phenomenon is closely associated with sweep and energetic inrush events, identified and described, respectively, by Corino and Brodkey[2] and Grass,[3] based on observations from similar visualization studies of the boundary-layer flow structure. The ejection and inrush events form linked parts of a random, cyclical process of turbulence generation in the boundary layer involving recurring instability. Grass[3] further clearly demonstrated the existence of both violent ejection and inrush events over rough walls. It was concluded that these were common features of boundary-layer turbulence irrespective of wall roughness condition.

The common presence of these dominant inrush and ejection structural features suggests that a shared mechanism could be responsible for their generation. Based on a combination of rational analysis and remarkable intuitive physical insight, Theodorsen[4] proposed a simple vortex model as the central element of the turbulence generation process in shear flows. This took the form of a horseshoe-shaped vortical structure inclined in the direction of mean shear illustrated in the author's original diagram reproduced in Fig. 1. Theodorsen conjectured, with extraordinary foresight in the light of evidence now emerging, that this vortex structure is a common feature of all shear layers, being present not only in wall-bounded flows but also in free shear layers, laminar to turbulent transition, and even sheared homogeneous turbulence.[5–18]

Kline and Robinson[19] presented a progress review of a community-wide cooperative study of boundary-layer structure that included an assessment and interpretation of recent numerical simulation studies of smooth wall flows. They drew the firm conclusion that powerful vortical structures, apparently representing rolled-up elements of typically incompletely developed and asymmetrical horseshoe form, represent the central feature of the turbulence generation process. Robinson[9] uses a very apt expression for the key role of these vortical structures, describing them as "pumps." The weight of existing evidence suggests that these vortical pumps are the primary agent for transport of mass, momentum, vorticity, heat, and other contaminants outwardly and inwardly across the boundary layer. They derive substantial energy from the mean flow by the simple mechanism of vortex stretching.

The overwhelming majority of boundary-layer turbulence structure investigations carried out to date relate to smooth wall flow. This is exclusively the case for the crucially important numerical simulation studies that can at present only cope with the simple smooth wall boundary condition. The investigations reported in the present paper concentrate attention on rough wall flows that more or less exclusively prevail in the geophysical environment. There is every reason to expect that horseshoe-type vortical structures also represent the dominant feature of boundary-layer structure over rough walls, and therefore the smooth wall observations remain highly relevant.

Results from two independent experimental studies are presented. For ease of reference these are simply termed experiment A and experiment B. The primary objective of experiment A was to try and establish the three-dimensional form of the turbulence structures linked to the ejection and inrush events observed over

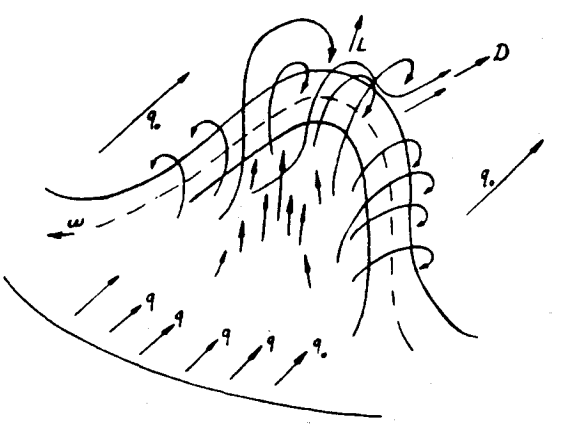

Fig. 1 Horseshoe vortex model first proposed by Theodorsen.[4]

Presented as Paper 91-0333 at the AIAA 29th Aerospace Sciences Meeting, Reno, NV, Jan. 7–10, 1991; received April 9, 1992; revision received Aug. 19, 1992; accepted for publication Aug. 31, 1992.

*Reader, Department of Civil and Environmental Engineering.

†Research Assistant, Department of Civil and Environmental Engineering; currently Senior Engineer, R. J. Brown Ltd., Perth, Australia.

‡Research Assistant, Department of Civil and Environmental Engineering.

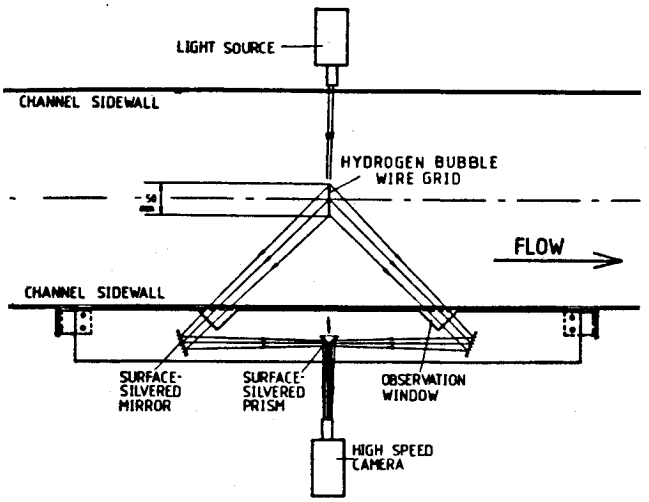

Fig. 2 Stereoscopic photographic system.

rough walls in the preceding investigation by Grass.[3] Based on the findings from this earlier study, Grass suggested that the near-wall turbulence structures should scale with the size of the wall roughness elements. Perry and Chong[20] adopted this suggestion in extending their hierarchy model to rough wall flows and scaling their first hierarchy of vortical structures in direct proportion to the roughness dimension. Experiment B is concerned with measuring the actual spanwise scale of the near-wall structures for boundary conditions ranging from hydrodynamically smooth to fully rough. This investigation also addresses the intriguing question of whether or not the equivalent of viscous sublayer streaks exists over rough walls.

A central objective of all of these basic studies is to provide an improved understanding of the fundamental physics of boundary-layer turbulence. Such knowledge is an essential prerequisite for the development of improved turbulence models. The success of this approach is demonstrated by the encouraging progress reflected in the models proposed, for example, by Perry et al.,[21] Walker et al.,[22] and Piomelli et al.[23]

Experimental Arrangements and Procedure

Experiment A

Measurements were made in a fully developed turbulent boundary layer formed on the rough bed of an open channel water flow. The glass-sided channel was 0.5 m wide and 6.2 m long, and the uniform flow depth was approximately 50 mm. Bed roughness comprised parallel spanwise strips of 5 mm square section brass rod, with a gap width of 20 mm, stuck to a glass bed plate. This produced k-type roughness.[24,25] The measurement station was located 2 m downstream from the leading edge of the bed plate at a position where the flow was fully developed but remained suitably two dimensional. A laser Doppler anemometer was used for the general control measurements and to obtain the mean velocity profile and long-term averaged turbulence characteristics.

The main emphasis of the experimental program centered on the successful design and deployment of a novel measurement system for approximate determination of the quasi-instantaneous velocity vector field throughout three-dimensional blocks of flow space. This technique was based on an adaptation of the hydrogen bubble tracer method previously described by Grass.[3] The single bubble-generating wire used in the earlier tests was replaced with an orthogonal grid comprised of 11 vertical and 12 horizontal 25-μ-diam wires in a vertical plane perpendicular to the flow direction. A negative voltage, pulsed at 20 Hz, was applied to the wire electrodes. This released 20 regular grid patterns of bubble tracers, comprising 132 node points into the flow every second. A high-speed motion camera running at 200 frames per second was used in conjunction with the stereoscopic viewing system illustrated in Fig. 2 to record the progress of the tracer grids as they were swept downstream. The hydrogen bubbles were illuminated by an intense narrow strip of light that ensured that only one tracer grid appeared in the field of view at any instant in time, to avoid visual confusion. The grid wire spacing was 5 mm, except in the zone of high velocity gradient close to the bed, where it was reduced to 2 mm in the vertical direction.

A film coordinate analyzer was used to measure the distance that the tracer grid node points moved in an interval of 1/100 s. These data were then processed by computer, making due allowance for perspective distortion and the wake velocity defect behind the generating wire (Grass[3]), to yield 132 simultaneously measured values of the three-dimensional velocity vector across a 50 × 50 mm area in the center of the channel. These velocity vector matrices were updated every 1/20 s, and Taylor's "frozen eddy" hypothesis was employed to generate an approximate picture of the quasi-instantaneous three-dimensional velocity field throughout blocks of the flow space swept through the measuring grid. The resulting three-dimensional velocity data matrix was then used to compute the corresponding vorticity field. This allowed vortex lines to be traced out through the three-dimensional flowfield as a powerful means of identifying the presence and delineating the geometry of vortical or other structural forms embedded in the boundary layer. A detailed description of the experimental arrangements and measurement techniques used in the experiment A study is given by Stuart.[26]

Experiment B

The experiment B test program was carried out using the same water channel and generally fully developed, uniform flow conditions as in experiment A, also maintaining the same flow depth of approximately 50 mm. The bed roughness condition was, however, varied in these tests from hydrodynamically smooth to fully rough. This was achieved using a range of different diameter glass spheres, packed in a single layer resting on the glass bed plate. Laser Doppler anemometry was again used for the general control measurements.

The main measurements, concerned with investigating the spanwise structure of the near-wall turbulence, once again employed the hydrogen bubble tracer technique. The general arrangement was, however, very much simpler than in experiment A and comprised a single, horizontal, bubble-generating wire located at variable height close to the bed. The bubble tracer lines were photographed through a viewing plate just touching the free water surface, using a still 35 mm camera. A coordinate analyzer was used to define the shape of the tracer lines in digital format for spacial spectrum analysis. Ensemble averages, based on 35 individual spectra, were calculated to establish the existence or otherwise of any preferred spanwise wavelength and to measure such wavelengths from the spectral peaks. The mean spacing of the low-speed streaks was also determined by direct measurement using a marking technique similar to that adopted by Smith and Metzler.[27] It was found that this method gave closely similar results, confirming that the two approaches are basically focusing on the same physical flow feature. The experiment B investigation was ongoing at the time of writing, and only preliminary results of direct relevance to the present discussion are presented in the next section.

Results and Discussion

Considering the experiment A results first, the long-term average mean velocity and normal and shear components of the Reynolds stresses were measured using a laser Doppler anemometer for comparison with previous work and to derive relevant scaling parameters. As expected, the two-dimensional strip roughness behaved as conventional k-type roughness, following the terminology and in-line with the findings of Perry and Joubert.[24] The measured streamwise and vertical components of turbulence intensity were in very close agreement with corresponding data obtained in similar open channel flows over beds with three-dimensional roughness elements by Grass,[3] Nezu,[28] and Raven.[29]

The mean velocity profile, measured in the center of the channel at the test location, is shown in relation to the bed roughness ele-

ments and the free water surface in Fig. 3. This particular set of data was measured above the centerline of one of the roughness strips. The effective velocity origin was determined using a combination of the progressive origin shift method suggested by Clauser[30] and adapted by Perry and Joubert[24] and linear regression to obtain the best fit straight line in the logarithmic zone. This procedure located the velocity origin 1.4 mm above the surface of the glass base plate and 3.6 mm below the tops of the roughness elements consistent with the findings of Perry and Joubert[24] and Perry et al.[25] The roughness length scale y_0 was derived from the intercept of the best fit logarithmic layer straight line with the y axis.

The bed shear stress and hence the bed shear velocity U_τ were obtained by extrapolating the linear total shear stress distribution, obtained by adding the Reynolds shear stress and viscous shear contributions, back to the bed. Derived values of the relevant scaling parameters and general flow and bed roughness characteristics are given in Table 1. If, following Nikuradse,[31] we consider an equivalent sand or, in the present case, gravel size k_s to produce the same degree of roughness, putting $y_0 = k_s/30 = 0.96$ mm (from Table 1), we find that $k_s/k = 5.74$ (where k denotes the roughness strip height = 5 mm). In comparison, the 12-mm-diam spherical roughness used in the experiment B tests yields a modest and expected k_s/k value of 0.82 (Table 1). These findings demonstrate that the two-dimensional strips produce a very rough boundary condition in line with previous study results.[32, 33]

Hydrogen bubble tracers generated on a single vertical wire were used for general dynamic flow visualization recorded using high-speed motion photography. All of the characteristic features of rough wall turbulence including violent eruptive ejection of fluid from the near-bed region and energetic inrush events bringing high-velocity fluid in toward the wall, observed in the earlier study using three-dimensional pebble roughness (Grass[3]) were clearly visible in the flow over the two-dimensional strip roughness. Roll-up of spanwise and streamwise vorticity was clearly apparent in the moving images as they developed in time.

The semimanual process used to abstract tracer coordinate data from the stereoscopic film images for the three-dimensional analysis was extremely time consuming. With the 132 node points and 20 Hz sampling rate used in the present study, it took approximately 20 h of film analysis time to generate three-dimensional data for 1 s of swept flow space. Set against this limitation, however, is the extraordinary power and potential of this novel technique that effectively generates data crudely equivalent to 132 triple-channel laser Doppler anemometers working simultaneously! It is undoubtedly the case that, linked to automated data acquisition systems, flow tracer methods such as the one presented here and alternative particle image velocimetry (PIV) approaches represent a feasible way forward to parallel developments in the numerical simulation area.

However, given the manually based techniques available in the present investigation, it was clearly essential to carefully select the blocks of swept flow space subjected to full three-dimensional

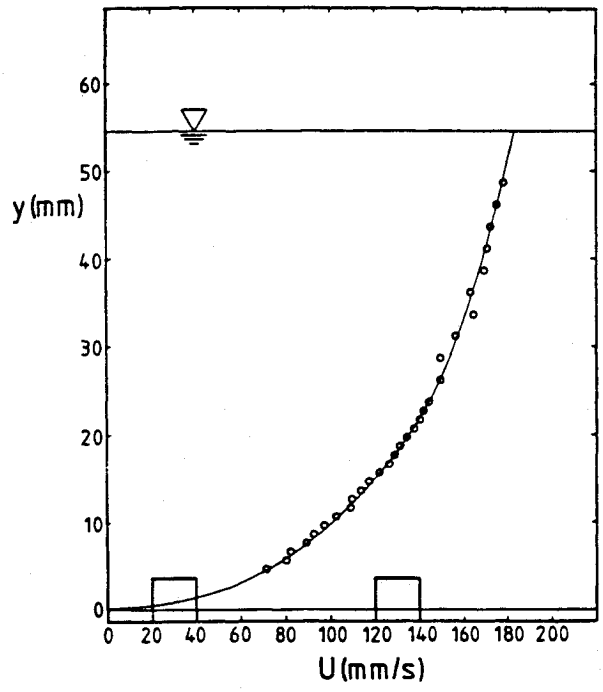

Fig. 3 Mean velocity profile in relation to the bed roughness elements and the free water surface.

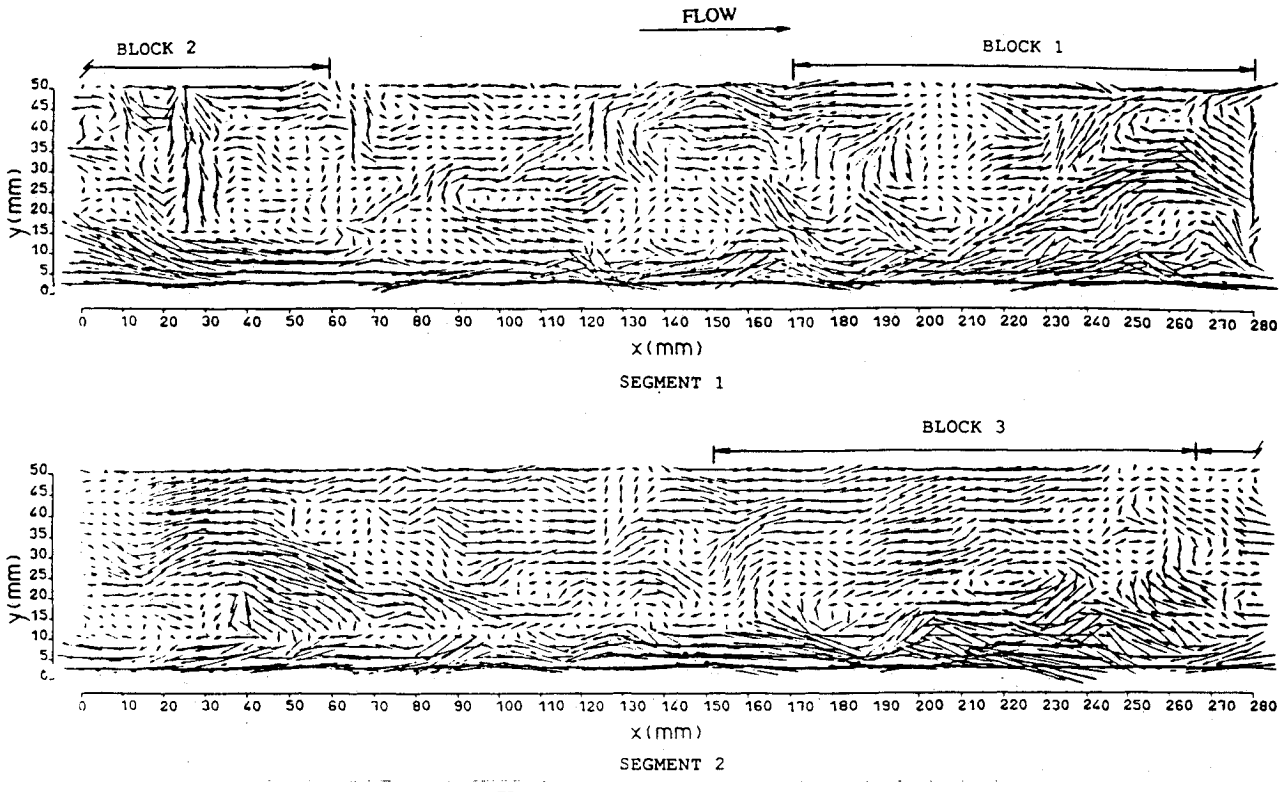

Fig. 4 Centerline ($u-U_c$, v) velocity vector plots in convected reference frame.

Table 1 Flow and bed roughness conditions and derived variables

Bed roughness condition	Experiment A	Experiment B			
	Two-dimensional strip roughness, $k = 5$ mm	Hydrodynamically smooth	Spherical roughness		
			$k = 1.15$ mm	$k = 6$ mm	k = 12 mm
Flow depth (relative to velocity origin D), mm	54.5	50.3	49.9	48.9	49.6
Depth-average velocity U, mm/s	144	105	106	111	106
Kinematic viscosity ν, mm^2/s	0.97	0.94	0.94	1.05	1.03
Reynolds number DU/ν	8076	5613	5611	5160	5114
Bed shear velocity U_τ, mm/s	16.1	6.07	6.46	8.48	9.21
Karman constant K	0.37	0.395	0.387	0.384	0.382
Roughness height					
k, mm	5	——	1.15	6	12
kU_τ/ν	83.0	——	7.9	48.5	107.3
Height of velocity origin above base plate datum, mm	1.4	——	0.70	4.8	9.4
Roughness length scale					
y_0, mm	0.96	——	0.025	0.169	0.327
$k_s = 30/y_0$	28.7	——	0.78	5.07	9.82
$k_s U_\tau/\nu$	476.4	——	5.4	40.9	79.2
k_s/k	5.74	——	0.68	0.85	0.82
Measurement height above roughness					
y_1, mm	——	1	1	3	3.5 0.5
λ, mm	——	15.6	16.1	19.5	38.2 12.0
$\lambda U_\tau/\nu$	——	101	110	158	340 107
λ/k	——	——	14.0	3.25	3.18 1.0

analysis to make best use of the severely restricted sampling time. Some method of previewing the general state of the flowfield was therefore required to establish periods when interesting events appeared to be occurring. This conditional sampling was achieved by initially carrying out a two-dimensional analysis, using the hydrogen bubble tracers released from the vertical centerline wire only, to measure instantaneous profiles of streamwise velocity u and vertical velocity v updated every 1/20 s. Taylor's hypothesis was then employed with an assumed convection velocity equal to the depth-averaged mean velocity $U_c = 144$ mm s^{-1}, obtained from the laser measurements, to generate $(u - U_c, v)$ vector plot segments of the type shown in Fig. 4. Five consecutive segments, each representing 2 s of flow time, 10 s in total, were considered.

The diagrams in Fig. 4 give a convected view impression of the instantaneous streamline patterns as seen by an observer traveling with the flow at the depth-averaged velocity U_c. Cross sections through transverse vortices of varying size and strength, inclined internal shear layers, and ejection and inrush zones are clearly visible in the flow structure. For example, note the vortex sections centered on segment 1 ($x = 145$ mm, $y = 20$ mm) and segment 2 ($x = 220$ mm, $y = 25$ mm); the shear layer located at segment 1 ($x = 240$ mm, $y = 30$ mm); and the ejection and inrush events located at segment 1 ($x = 10$ mm, $y = 10$ mm) and segment 2 ($x = 270$ mm, $y = 5$ mm), respectively. The original versions of the velocity vector diagrams in Fig. 4 were color coded according to whether the local streamwise velocity component was greater or less than the local mean value. Ejection events thus appeared as black and inrush events as red groupings of velocity vectors. Identification of these dominant Reynolds shear stress and turbulence production events in the Fig. 4 segments was also facilitated by inspection of the instantaneous Reynolds shear stress profiles calculated from the instantaneous (u, v) velocity distributions.

Three sections of the Fig. 4 velocity vector segments were selected on the basis of apparently relevant structural content for full three-dimensional analysis. These are referred to as blocks 1, 2, and 3 (Fig. 4). With reference to the previously quoted examples, block 1 includes the segment 1 shear layer structure; block 2, the segment 1 ejection event, which is linked to high measured Reynolds shear stress; and block 3, the segment 2 vortex section associated with an extremely active, underlying ejection zone at the bed.

The block 1 shear layer can be directly compared with a corresponding velocity vector representation of a similar structure presented by Robinson et al.[34] and derived from numerical circulation of a turbulent boundary layer formed on a smooth wall. The detailed matching between these two flowfield patterns is quite remarkable, with the velocity vectors surrounding the rolled-up vortex head and the upstream stagnation point closely reproduced in both direction and magnitude. This certainly suggests a close identity between the three-dimensional flow structures generating these velocity patterns over a completely smooth and a fully rough boundary. The fact that the general flow pattern associated with the shear layers illustrated in Fig. 4 also recurs in the ensemble averaged patterns of the large-scale structure produced by Thomas and Brown,[35] for example, adds support to the concept of a vortical generating structure of basically universal geometry, but following a scale hierarchy, as suggested by Perry and Chong.[20]

It is apparent from the previous discussion that two-dimensional velocity vector representations on sliced planes through the flowfield are extremely effective in revealing the presence and form of relevant structural features. The three-dimensional analysis provided three-component velocity vector data throughout the swept volumes of blocks 1, 2, and 3. This permits a whole series of velocity vector plots to be produced for different vertical streamwise, vertical crossflow, and horizontal planes. Examples of these slice representations of the velocity field are shown in Fig. 5 for the block 2 results. Because of the vertical mean velocity gradient, it is necessary to vary the convection velocity for the plots in the horizontal (x, z) plane. It was found that using the mean streamwise velocity at the level of the plane height above the bed gave satisfactory results as indicated in Fig. 5b. Once again vortex sections can be identified in all three planes. These three-dimensional rep-

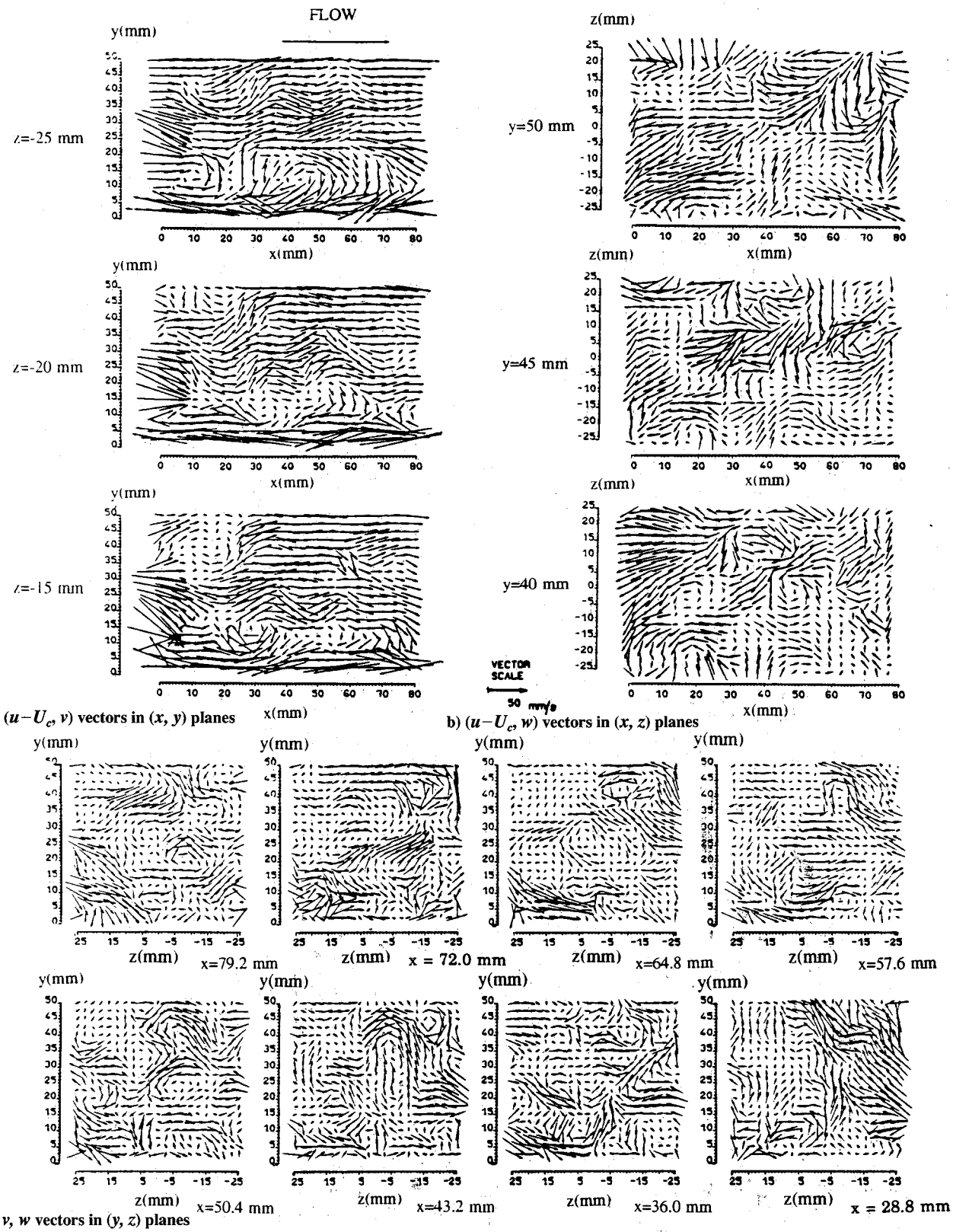

Fig. 5 Examples of velocity vector plots from three-dimensional block 2.

resentations are additionally valuable since they permit assessment of the extent of spacial coherence in the observed structures. The original plots were again color coded to identify zones where the streamwise velocity component was either greater or less than the local mean velocity.

The block 2 vorticity field was explored first. This was carried out in a comprehensive and systematic manner, initially ignoring the information obtained from the velocity vector plots concerning the presence, form, and location of any coherent structure. Single vortex lines were tracked from over 200 starting points spread in a regular grid pattern throughout the block. Examples of these vortex lines with starting points located in horizontal planes 7.5, 15, and 30 mm above the tops of the roughness strips are presented in Fig. 6. The most surprising feature of these single vortex lines is their extraordinary coherent, untangled form. This finding is particularly surprising if one observes the apparently relatively advanced state of chaos existing in the near-wall flowfield as recorded by the general flow visualization films. Dominant vortic-

ity in the flowfield is clearly associated with relatively young and coherent flow structures. Vortex lines transported long distances in old contorted structures would presumably exhibit a much more tangled form. Although examples of tangled vortex lines were found among the very large sample, they represented a small percentage, and the vortex lines in Figs. 1–3 are typical. The fact that the vortex lines often span between the wall and the flow surface and yet remain within the confines of the measurement volume under the action of the velocity gradient suggests that the transport across the boundary layer has been relatively rapid. It also suggests that the structures responsible for such transport must be of a scale commensurate with the boundary-layer thickness or flow depth.

To give a clearer impression of the three-dimensional form of the vortex lines, their projected images are plotted on the block side walls and base. As expected, the side wall projections invariably indicate downstream inclination that in turn implies strong vortex stretching and energy absorption from the mean flowfield. Horseshoe-shaped loops are also very common features of these single vortex lines. Although such features can be formed by a lifted shear layer and may not be indicative of a rolled-up horseshoe vortex, they can be taken as a possible indication of the presence and location of such structures for further investigation using multiple vortex lines. Such lines also represent a Lagrangian, integrated history of the movement of the fluid particles constituting the line, or in its near vicinity, subsequent to their being lifted away from the vorticity generating zone at the wall (Lighthill[36]). Even in a passive role as flow tracer, therefore, vortex lines give valuable information about the recent local structure of the flow. Perhaps the most significant qualitative impression given by these single vortex lines, typically illustrated in Fig. 6, is of a flow dominated by coherent powerful new structures that all connect back to the wall and that increase in size with wall distance. This observation is entirely consistent with Townsend's attached eddy hypothesis used as a basis for their model by Perry and Chong.[20]

The fact that many of these looping, single vortex lines are embedded in rolled-up vortical structures was demonstrated by multiple line tracking. The resulting vortex line bundles are shown in Figs. 7c and 7d, which correspond to Figs. 6a and 6b. The splendid example of a near-bed, horseshoe vortex in Fig. 7d is directly linked to the ejection event located at coordinate point (x = 10 mm,

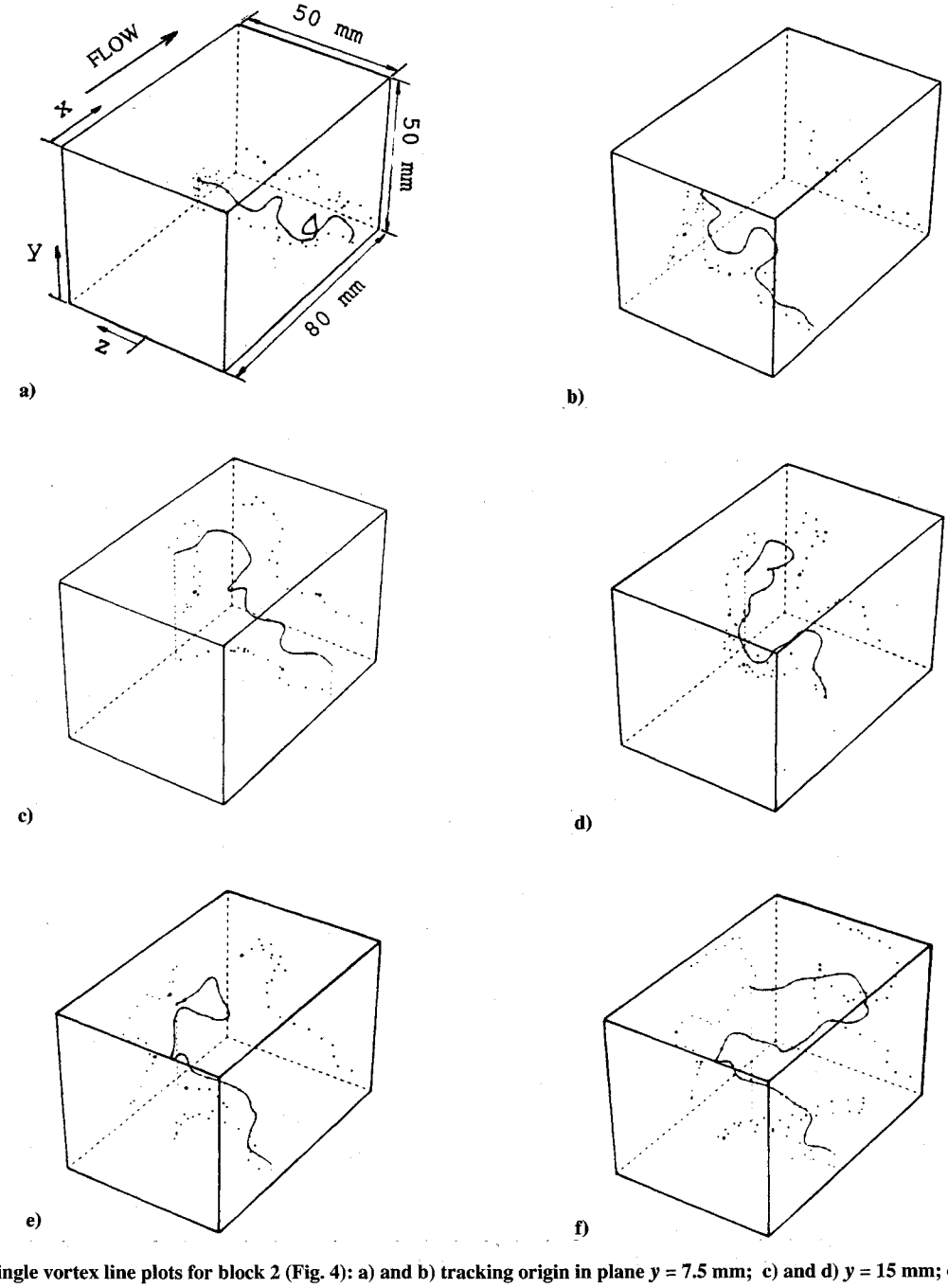

Fig. 6 Typical single vortex line plots for block 2 (Fig. 4): a) and b) tracking origin in plane y = 7.5 mm; c) and d) y = 15 mm; e) and f) y = 30 mm.

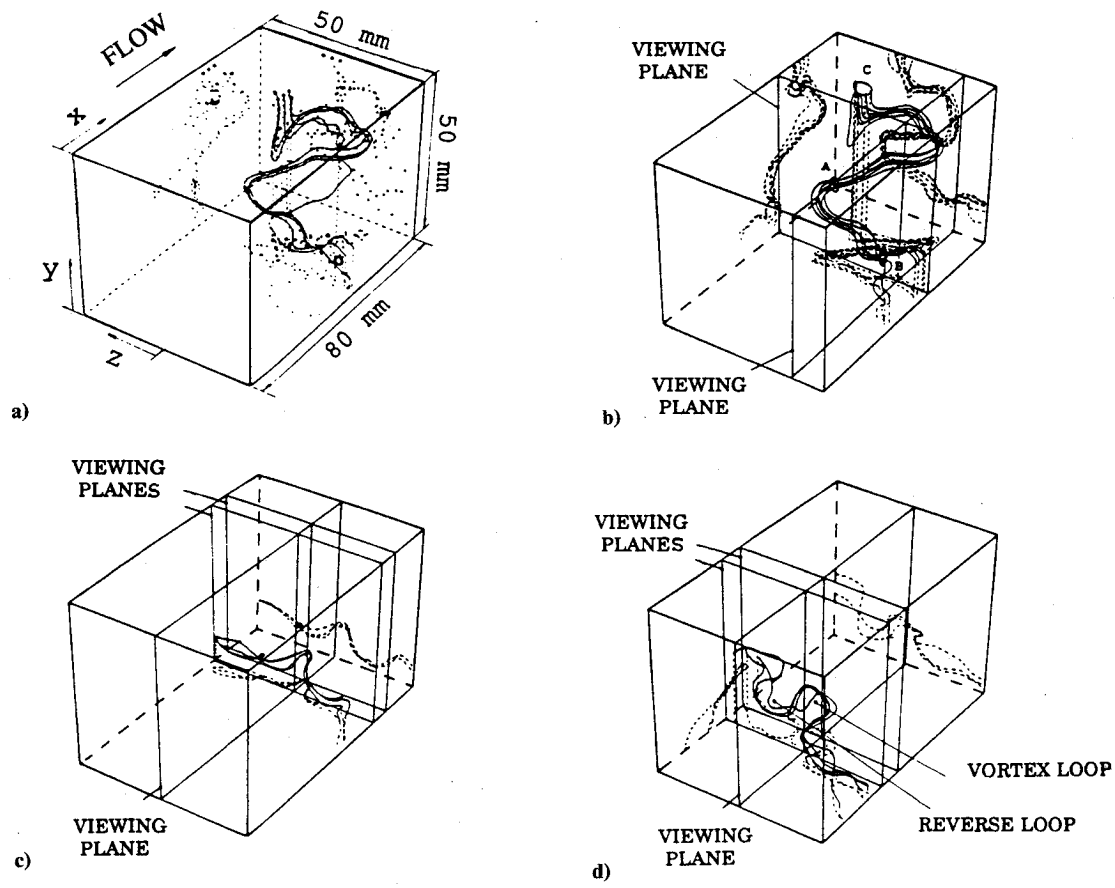

Fig. 7 Multiple vortex line plots revealing vortical structures embedded in the block 2 flowfield (Fig. 4).

$y = 10$ mm) in segment 1, Fig. 4. This ejection event is also marked by the outward (v, w) velocity vectors in the crossflow plane located at $x = 36$ mm, $y = 10$ mm, $z = 0$ mm in Fig. 5c. Fluid is being pulled up and ejected between the side legs of this horseshoe vortex.

The spectacular snaking vortex displayed in Figs. 7a and 7b loops its way upward across the entire thickness of the boundary layer and terminates in a loose, broken end at the free surface. Whirlpool marks are a commonly observed surface feature of river flows and undoubtedly result from the draw down effect of such free vortex ends.[3,10,37] Vortex cross sections marked A, B, and C in Fig. 7b are discernible in the velocity vector plots in Fig. 5. Streamwise cross-section A is located at approximate coordinate position ($x = 50.4$ mm, $y = 25$ mm, and $z = -5$ mm) in Fig. 5c, spanwise cross-section B at ($x = 30$ mm, $y = 15$ mm, and $z = -15$ mm) in Fig. 5a, and the free-surface horizontal cross section at ($x = 70$ mm, $y = 50$ mm, and $z = 5$ mm) in Fig. 5b. This strong correlation and coincidence between vortex line and velocity vector representations reinforces confidence in the reality of these vortical structures.

Further examples of multiple vortex line displays are presented in Fig. 8. Once again these plots demonstrate clear coherence in the flow structure and provide additional direct evidence of the presence of vortical structures with a general horseshoe-type configuration and with a wide range of scales. The plots in Figs. 8a–8d are for block 1, which was selected for three-dimensional analysis because of the interesting shear layer revealed by the centerline velocity vector plots (Fig. 4). The vortex lines shown in Fig. 8b collectively trace out the general shape of a horseshoe vortex with a powerful streamwise limb indicated by the necked region. This vortex is associated with the strong eruption of wall layer fluid reflected by the sharp spanwise inclination in the shear layer vortex lines illustrated in Figs. 8c and 8d.

Block 3 was selected for three-dimensional analysis on the basis of the vortex cross section identified at position $x = 220$ mm, $y = 25$ mm in segment 2 of Fig. 4 and the active underlying ejection zone. The three-dimensional velocity vector diagrams and the vortex line bundle presented in Fig. 8f show that the parent vortex spans the entire block width and takes the form of a looped structure arching upward from the wall. This is directly linked to strong ejection events and associated high Reynolds stress production just upstream of the vortex. Evidence of other horseshoe-shaped vortical structures embedded in the block 3 flow space is presented in Figs. 8e, 8g, and 8h.

To conclude this discussion of the experiment A results therefore, it is self-evident that the presence of vortical structures such as those depicted, for example, in Figs. 7b and 8b, with their massive potential for absorption of mean flow energy through the stretching mechanism and their capacity to induce strong three-dimensional currents and hence generate large contributions to Reynolds shear stress, must play a critical role in turbulent boundary-layer dynamics. This key role has perhaps been best summed up by Kuchemann,[38] who described vortices as "the sinews and muscles of fluid motion."

Turning now briefly to the preliminary experiment B results, the general flow conditions and values of derived parameters such as the bed shear velocity U_τ and the roughness length scale y_0 are set out in Table 1. Roughness Reynold's numbers $U_\tau k/\nu$ are also quoted in Table 1 and indicate that, under these particular flow conditions, the 1.15-mm-diam spheres lie in the lower transitional roughness regime, the 6-mm spheres in the upper transitional regime, and the 12-mm spheres in the fully rough regime.

The smooth wall visualization photograph in Fig. 9a clearly illustrates the extensive coherence of the low-speed streaks in the streamwise direction. Similar coherence is seen to persist for the 1.15-mm-diam roughness (Fig. 9b) reflecting the continued dominance of viscous shear transfer at the wall. These low velocity ejection zones are still apparent in the near-wall layer flow over the 6-mm-diam spheres. However, as illustrated in Fig. 9c, their general characteristics have now changed significantly. The distance between the zones has clearly increased as has their width, whereas their streamwise coherence is substantially reduced.

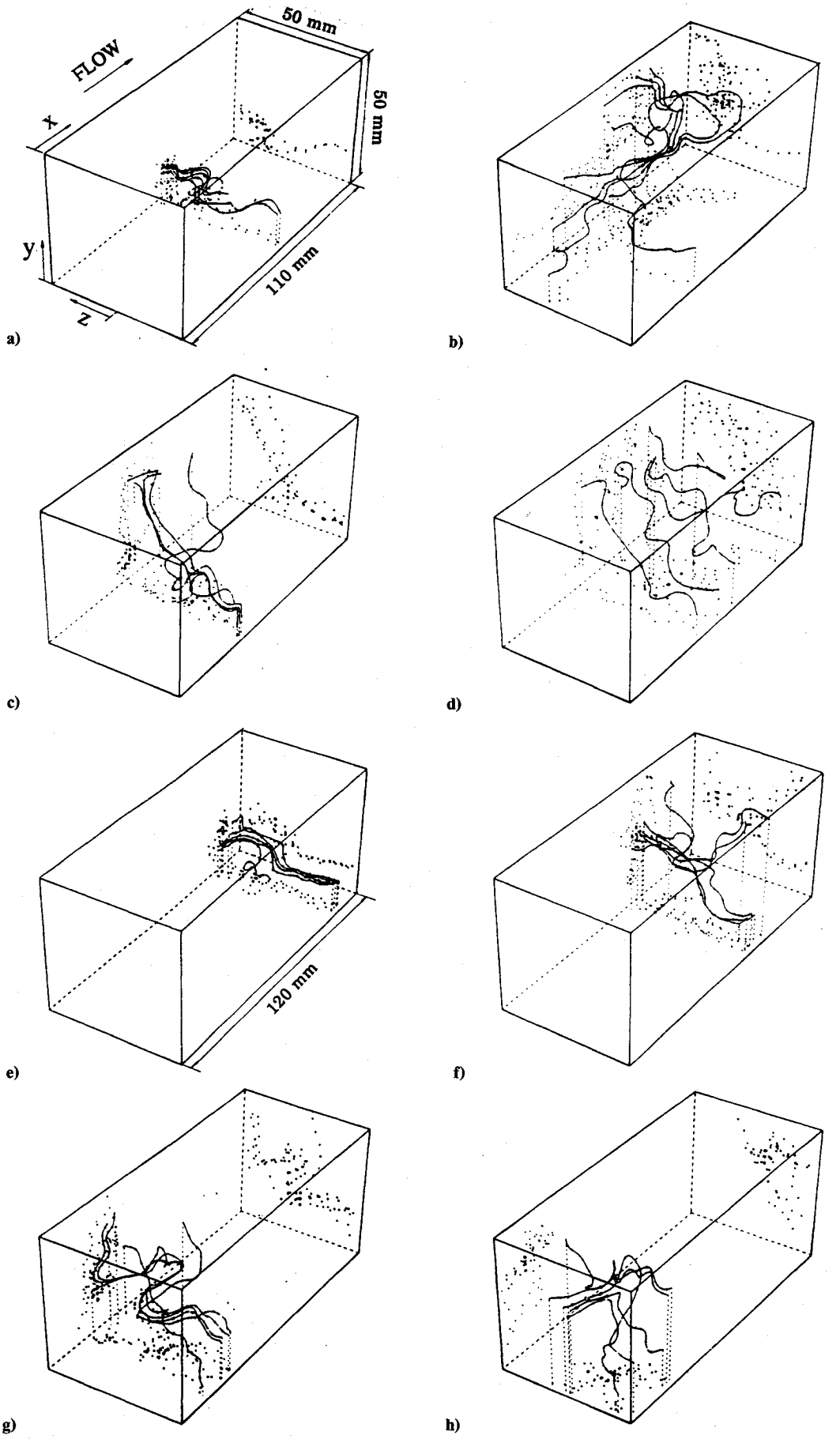

Fig. 8 Multiple vortex line plots revealing vortical and coherent structures in blocks 1 (Figs. 8a–8d) and 3 (Figs. 8e–8h) (Fig. 4) flowfield.

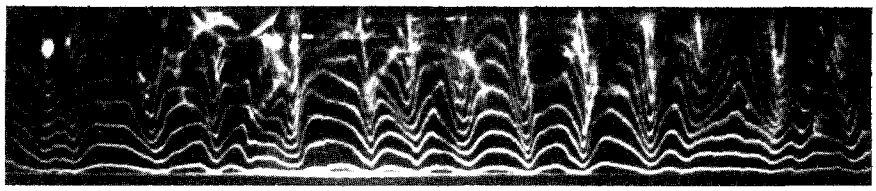

a) Smooth: $y_1 = 1$ mm

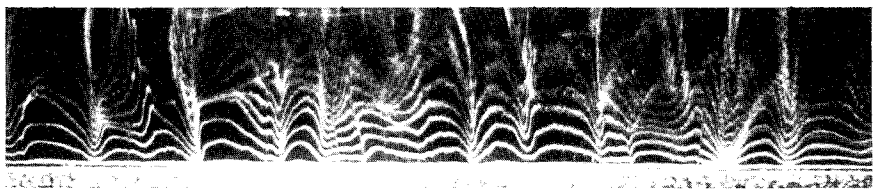

b) $k = 1.15$ mm, $y_1 = 1$ mm

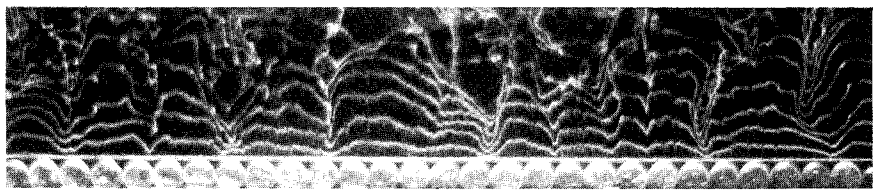

c) $k = 6$ mm, $y_1 = 3$ mm

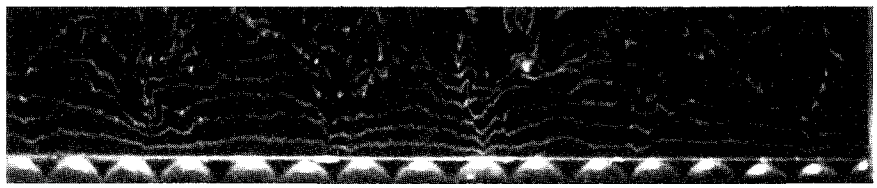

d) $k = 12$ mm, $y_1 = 3.5$ mm

e) $k = 12$ mm, $y_1 = 0.5$ mm

Fig. 9 Near wall flow structure visualized by hydrogen bubble tracers generated on spanwise wire parallel to the bed. Bed roughness conditions and wire distance from top of roughness y_1.

These trends are further advanced in the case of the fully rough 12-mm-diam spheres.

A remarkable feature of the rough wall flow is its apparent ability to order itself very rapidly over a small vertical distance above the tops of the roughness elements. This is demonstrated by contrasting the near-bed flowfield characteristics visualized in Figs. 9d and 9e. In Fig. 9e, the hydrogen bubble wire is located 0.5 mm above the tops of the spheres. At this height the bubble tracers respond to the three-dimensional velocity field and pick up the intense small-scale disturbances in the separating flow round the individual roughness elements. The visualization traces show very little evidence of this highly disturbed flow state with the wire raised to just 3 mm above the tops of the 12-mm-diam spheres as shown in Fig. 9d.

Ensemble-averaged spectra for the spanwise velocity fluctuations, corresponding to the mean flow and bed roughness conditions in Figs. 9a–9e are presented in Figs. 10a–10e. As can be seen, these spectra exhibit a well defined single peak that indicates the presence of a dominant spanwise wavelength λ in the near-wall structure. The ability of the spectral peak method to pick out a preferred wavelength in the velocity perturbations is confirmed by the measured value of 12 mm with the hydrogen bubble wire 0.5 mm above the roughness tops as in Fig. 10e. This wavelength exactly coincides with the sphere diameter as expected. In the case of the smooth wall flow, $\lambda^+ = \lambda U_\tau / \nu = 101$, in good agreement with previous measurements.[1,27]

For the roughness Reynolds numbers quoted in Table 1, under the present test conditions, λ should be largely independent of Reynolds number for the 6- and 12-mm-diam roughness elements. In these circumstances, following the suggestion of Grass,[3] λ should scale with the roughness dimension k. In other words, λ/k = const for the geometrically similar roughness elements and packing used in these tests. This expectation is closely confirmed with measured λ/k values of 3.25 and 3.18 for the 6- and 12-mm spheres, respectively (Table 1). A primary objective of this continuing investigation is to more fully explore the mechanisms responsible for generating these preferential spanwise wavelengths in the near- wall layers.

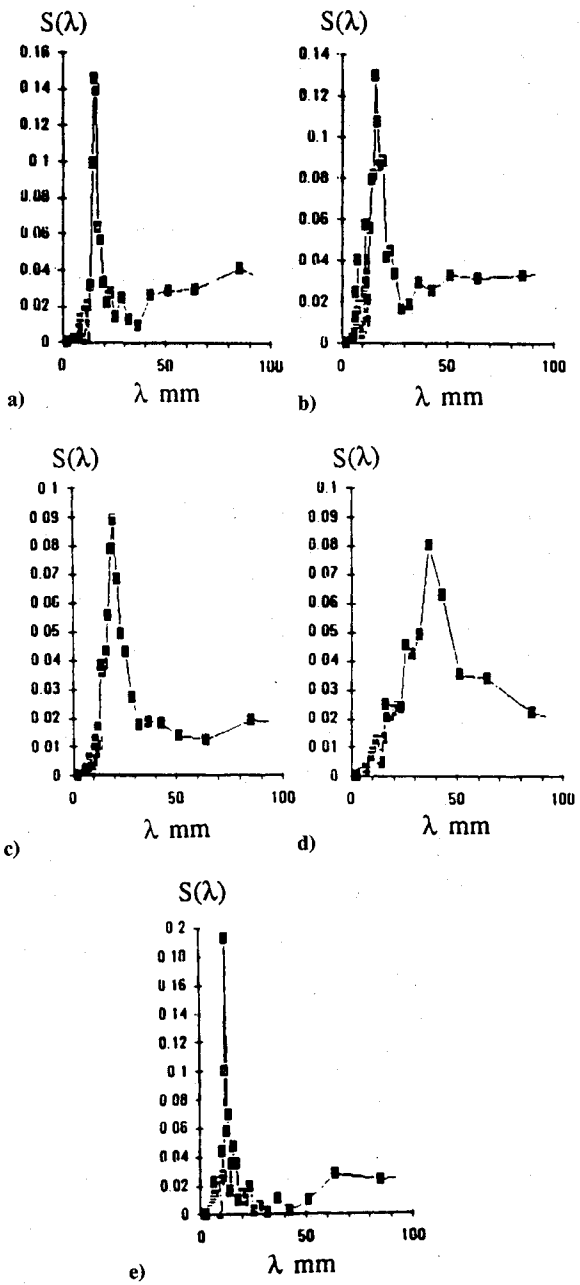

Fig. 10 Ensemble averages of wavelength spectra of spanwise velocity fluctuations derived from hydrogen bubble tracers as illustrated in Fig. 9. Flow conditions and y_1 values of Figs. 10a–10e correspond to Figs. 9a–9e, respectively.

Conclusions

There is now convincing evidence, particularly from recent direct numerical simulation studies, that horseshoe-type vortical structures, usually with an asymmetrical or partially rolled-up form, represent the dominant element in smooth wall boundary-layer turbulence. These vortices act as pumps transporting mass, momentum, vorticity, and contaminants, passive or otherwise, across the boundary layer.

The present results from the experiment A test program provide evidence, based for the first time on direct physical measurements of the three-dimensional vorticity field, that horseshoe vortical structures are present and play an equally important role in rough wall flows.

Preliminary results from the experiment B investigation show that, just as in the case of the viscous sublayer region of smooth wall flow, a dominant spanwise wavelength occurs in the instantaneous crossflow distribution of streamwise velocity close to the rough wall. The measurements indicate that for fully rough wall conditions this wavelength, which reflects the typical scale of near-wall vortical structures, is directly proportional to the bed roughness size.

The area of greatest remaining uncertainty in our knowledge and understanding of the physics of boundary-layer turbulence concerns the process of growth in scale up through the eddy hierarchy from the often diminutive wall scales to the very large outer layer scales. Further work is needed at high geophysical scale Reynold's numbers and on the fundamentals of vortex interaction and vorticity field development under shear straining conditions.

Acknowledgment

The authors wish to acknowledge the support of the Science and Engineering Research Council for a major part of the reported investigation.

References

[1]Kline, S. J., Reynolds, W. C., Schraub, F. A., and Runstadler, P. W., "The Structure of Turbulence in Boundary Layers," *Journal of Fluid Mechanics*, Vol. 30, 1967, pp. 741–773.

[2]Corino, E. R., and Brodkey, R. S., "A Visual Investigation of the Wall Region in Turbulent Flow," *Journal of Fluid Mechanics*, Vol. 37, 1969, pp. 1–30.

[3]Grass, A. J., "Structural Features of Turbulent Flow Over Smooth and Rough Boundaries," *Journal of Fluid Mechanics*, Vol. 50, 1971, pp. 233–255.

[4]Theodorsen, T., "Mechanism of Turbulence," *Proceedings of the 2nd Midwestern Conf. on Fluid Mechanics,* Ohio State Univ., Columbus, OH, 1952, pp. 1–18.

[5]Moin, P., and Kim, J., "Numerical Investigation of Turbulent Channel Flow," *Journal of Fluid Mechanics,* Vol. 118, 1982, pp. 341–377.

[6]Moin, P., and Kim, J., "The Structure of the Vorticity Field in Turbulent Channel Flow: Part 1, Analysis of Instantaneous Fields and Statistical Correlations," *Journal of Fluid Mechanics*, Vol. 155, 1985, pp. 441–464.

[7]Kim, J., and Moin, P., "The Structure of the Vorticity Field in Turbulent Channel Flow: Part 2, Study of Ensemble-Averaged Fields," *Journal of Fluid Mechanics*, Vol. 162, 1986, pp. 339–363.

[8]Wallace, J. M., "The Vortical Structure of Bounded Turbulent Shear Flow," *Lecture Notes in Physics,* 235, Springer-Verlag, Berlin, 1985, pp. 253–268.

[9]Robinson, S. K., "A Review of Vortex Structures and Associated Coherent Motions in Turbulent Boundary Layers," Second IUTAM Meeting on Structure of Turbulence and Drag Reduction, Zurich, Switzerland, July 1989.

[10]Muller, A., and Gyr, A., "On the Vortex Formation in the Mixing Layer Behind Dunes," *Journal of Hydraulic Research,* Vol. 24, No. 5, 1986, pp. 359–375.

[11]Sene, K. J., Thomas, N. H., and Goldring, B. T., "Planar Plunge-Zone Flow Patterns and Entrained Bubble Transport," *Journal of Hydraulic Research*, Vol. 27, No. 3, 1989, pp. 363–383.

[12]Ferre, J. A., Mumford, J. C., Savill, A. M., and Giralt, F., "Three-Dimensional Large-Eddy Motions and Fine-Scale Activity in a Plane Turbulent Wake," *Journal of Fluid Mechanics*, Vol. 210, 1990, pp. 371–414.

[13]Hama, F. R., and Nutant, J., "Detailed Flow-Field Observations in the Transition Process in a Thick Boundary Layer," *Proceedings of the 1963 Heat Transfer and Fluid Mechanics Institute,* Stanford Univ. Press, Stanford, CA, 1963, p. 77.

[14]Williams, D. R., Fasel, H., and Hama, F. R., "Experimental Determination of the Three-Dimensional Vorticity Field in the Boundary-Layer Transition Process," *Journal of Fluid Mechanics*, Vol. 149, 1984, pp. 179–203.

[15]Acalar, M. S., and Smith, C. R., "A Study of Hairpin Vortices in a Laminar Boundary Layer: Part 1, Hairpin Vortices Generated by Hemispherical Protuberances," *Journal of Fluid Mechanics*, Vol. 175, 1987, pp. 1–41; "Part 2, Hairpin Vortices Generated by Fluid Injection," *Journal of Fluid Mechanics*, Vol. 175, 1987, pp. 43–83.

[16]Perry, A. E., Lim, T. T., and Teh, E. W., "A Visual Study of Turbulent Spots," *Journal of Fluid Mechanics*, Vol. 104, 1981, pp. 387–405.

[17]Rogers, M. M., and Moin, P., "The Structure of the Vorticity Field in Homogeneous Turbulent Flows," *Journal of Fluid Mechanics*, Vol. 176, 1987, pp. 33–66.

[18]Lee, M. J., Kim, J., and Moin, P., "Structure of Turbulence at High Shear Rate," *Journal of Fluid Mechanics*, Vol. 216, 1990, pp. 561–583.

[19]Kline, S. J., and Robinson, S. K., "Turbulent Boundary Layer Structure: Progess, Status and Challenges," Second IUTAM Meeting on Structure of Turbulence and Drag Reduction, Zurich, Switzerland, July 1989.

[20]Perry, A. E., and Chong, M. S., "On the Mechanism of Wall Turbu-

lence," *Journal of Fluid Mechanics*, Vol. 119, 1982, pp. 173–217.

[21]Perry, A. E., Henblest, S., and Chong, M. S., "A Theoretical and Experimental Study of Wall Turbulence," *Journal of Fluid Mechanics*, Vol. 165, 1986, pp. 163–199.

[22]Walker, J. D. A., Abbott, D. E., Schnarnhorst, R. K., and Weigand, G. G., "Wall-Layer Model for the Velocity Profile in Turbulent Flows," *AIAA Journal*, Vol. 27, No. 2, 1989, pp. 140–149.

[23]Piomelli, U., Ferziger, J., and Moin, P., "New Approximate Boundary Conditions for Large Eddy Simulations in Wall-Bounded Flows," *Physics of Fluids A*, Vol. 1, No. 6, 1989, pp. 1061–1068.

[24]Perry, A. E., and Joubert, P. N., "Rough Wall Boundary Layers in Adverse Pressure Gradients," *Journal of Fluid Mechanics*, Vol. 17, 1963, pp. 193–211.

[25]Perry, A. E., Schofield, W. H., and Joubert, P. N., "Rough Wall Turbulent Boundary Layers," *Journal of Fluid Mechanics*, Vol. 37, 1969, pp. 383–413.

[26]Stuart, R. J., "Three-Dimensional Characteristics of Coherent Flow Structures in a Turbulent Boundary Layer Over a Rough Surface," Ph.D. Dissertation, Univ. of London, London, England, UK, 1984.

[27]Smith, C. R., and Metzler, S. P., "The Characteristics of Low-Speed Streaks in the Near-Wall Region of a Turbulent Boundary Layer," *Journal of Fluid Mechanics*, Vol. 129, 1983, pp. 27–54.

[28]Nezu, I., "Turbulence Intensities in Open Channel Flows," *Proceedings of the Japan Society of Civil Engineers*, Vol. 261, 1977, pp. 67–76.

[29]Raven, P. W. J., "Turbulent Boundary Layer Characteristics in Open Channel Flow over Fixed and Mobile Sand Beds," Ph.D. Dissertation, Univ. of London, London, England, UK, 1977.

[30]Clauser, F. H., "Turbulent Boundary Layer," *Advances in Applied Mechanics*, Vol. IV, 1956, p. 1.

[31]Nikuradse, J., "Stromungsgesetze in Rauhen Rohren," *Ver. deutsch. Ing. Forschungsheft*, No. 361, 1933.

[32]Yaglom, A. M., "Similarity Laws for Constant-Pressure and Pressure-Gradient Turbulent Wall Flows," *Annual Review of Fluid Mechanics*, Vol. 11, 1979, pp. 505–540.

[33]Paeschke, W. "Experimentelle Untersuchungen zum Rauhigkeits-und Stabilitatsproblem in der bodennahen huftschicht," *Beitr. Phys. fr. Atmos.*, Vol. 24, 1937, pp. 163–189.

[34]Robinson, S. K., Kline, S. J., and Spalart, P. R., "A Review of Quasi-Coherent Structures in a Numerically Simulated Turbulent Boundary Layer," NASA TM 102191, May 1989.

[35]Thomas, A. S. W., and Brown, G. L., "Large Structure in a Turbulent Boundary Layer," 6th Australasian Hydraulics and Fluid Mechanics Conf., Adelaide, Australia, Dec. 1977.

[36]Lighthill, M. J., "Waves and Hydrodynamic Loading," *Proceedings of the Second International Conf. on the Behavior of Off-Shore Structures* (London, England), BHRA Fluid Engineering, Cranfield, England, UK 1979, pp. 1–40.

[37]Jackson, R. G., "Sedimentological and Fluid-Dynamic Implications of the Turbulent Bursting Phenomenon in Geophysical Flows," *Journal of Fluid Mechanics*, Vol. 77, 1976 , pp. 531–560.

[38]Kuchemann, D., "The I.U.T.A.M. Symposium on Concentrated Vortex Motions in Fluids," *Journal of Fluid Mechanics*, Vol. 21, 1965, pp. 1–20.